INSTITUTE OF PHYSICS PUBLISHING JOURNAL OF PHYSICS D: APPLIED PHYSICS

J. Phys. D: Appl. Phys. **39** (2006) 2979–2992 doi:10.1088/0022-3727/39/14/017

Diffusion correction to the Raether–Meek criterion for the avalanche-to-streamer transition

Carolynne Montijn[1] **and Ute Ebert**[1,2]

[1] CWI, PO Box 94079, 1090 GB Amsterdam, The Netherlands
[2] Department of Physics, Eindhoven University of Technology, Eindhoven, The Netherlands

Received 22 December 2005, in final form 26 April 2006
Published 30 June 2006
Online at stacks.iop.org/JPhysD/39/2979

Abstract
Space-charge dominated streamer discharges can emerge in free space from single electrons. We reinvestigate the Raether–Meek criterion and show that streamer emergence depends not only on ionization and attachment rates and gap length, but also on electron diffusion. Motivated by simulation results, we derive an explicit quantitative criterion for the avalanche-to-streamer transition both for pure non-attaching gases and for air, under the assumption that the avalanche emerges from a single free electron and evolves in a homogeneous field.

(Some figures in this article are in colour only in the electronic version)

1. Introduction

1.1. Problem setting and review

Emergence and propagation of streamer-like discharges are topics of current interest. Streamers play a role in creating paths for sparks and lightning [1,2] and in sprite discharges at high altitude above thunderclouds [3–5]. They are also used in various industrial applications [6], e.g. in corona reactors for water and gas treatment [7–10] and as sources of excimer radiation for material processing [11–13], for a recent overview see [14].

In the present paper, we investigate the conditions under which a tiny ionization seed like a single electron grows out into a streamer with self-induced space charge effects and consecutive rapid growth; we assume that the electric field is homogeneous and that electrodes are so far away that they play no role. The critical length or time for this transition as a function of the electric field is usually described by the Raether–Meek criterion. We will confront recent simulation results with the underlying assumptions of the Raether–Meek criterion and then derive a diffusion correction to it. This correction can amount to a factor of 2 or more for transition time and length for certain parameters as we will elaborate below and summarize in figures 5 and 6. In non-attaching gases the consequences are particularly severe since in low fields the diffusion can suppress streamer formation almost completely while the Raether–Meek criterion would predict streamer formation after a finite travel distance and time. An example of such an avalanche in extremely low fields is discussed in [15].

In many applications, discharges are enclosed by containers and electrodes; streamers then frequently emerge from point or rod electrodes that create strong local fields in their neighbourhood [16] and also influence the discharge by surface effects. On the other hand, in many natural discharges and, in particular, for sprites above thunderclouds [5], it is appropriate to assume that the electric field is homogeneous and metal electrodes are absent. In this case, single electrons can create ionization avalanches that move into the electron drift direction. From those avalanches, single or double ended streamers can emerge [17, 18], and we are interested in the prediction of this transition. For clarity, we call a spatial distribution of charged particles an avalanche, if the electric field generated by their space charges is negligible in comparison with the background external field; on the other hand, if the space charges of the distribution substantially contribute to the total field, we speak of a streamer.

The critical field required for lightning generation is presently a topic of debate, in particular, whether thundercloud fields are sufficient for classical breakdown or whether relativistic particles from cosmic air showers are required [19, 20]. Different critical fields can be defined for different processes; for example, in [16] a critical field for positive streamer propagation is suggested that is valid after the streamers have emerged from a needle electrode. This field is certainly lower than the critical field for streamer emergence from an avalanche to be discussed here.

Of course, dust particles or other nucleation centres can play an additional role in discharge generation in thunderclouds, but in the present paper we will focus on the effect of a homogeneous field in a homogeneous gas. This situation corresponds to the classical experiments of Raether in the thirties of the last century [21].

In this introductory and motivating section, we first recall the common discharge model and present simulation results for avalanches and consecutive streamers that emerge from a single electron in a homogeneous field far from any surfaces. Then we recall the Raether–Meek criterion; it suggests that the avalanche to streamer transition depends on the ionization rate α and gap length d through the dimensionless combination αd. We confront this criterion with our simulations and argue that the transition depends not only on the product of ionization coefficient and gap length but also on electron diffusion. Now numerical evaluations of the initial value problem for a large range of parameters, namely fields, gas types and densities, would be very tedious. However, we have succeeded in making analytical progress on the transition criterion. This has two major advantages: first, general expressions for arbitrary fields, gases and densities can be derived. Second, the result can be given in the form of a closed mathematical expression. These calculations and results form the body of the paper.

1.2. Discharge model and simulation results

To be specific, we consider a continuous discharge model with attachment and local field-dependent impact ionization rate and space charge effects. It is defined through

$$\partial_t n_e = \nabla_{\boldsymbol{R}} \cdot (D_e \nabla_{\boldsymbol{R}} n_e + \mu_e \boldsymbol{E} n_e) + (\mu_e |\boldsymbol{E}| \alpha_i(|\boldsymbol{E}|) - \nu_a) n_e, \tag{1}$$

$$\partial_t n_+ = \mu_e |\boldsymbol{E}| \alpha_i(|\boldsymbol{E}|) n_e, \tag{2}$$

$$\partial_t n_- = \nu_a n_e, \tag{3}$$

$$\nabla_{\boldsymbol{R}}^2 \Phi = \frac{\mathrm{e}}{\epsilon_0}(n_e + n_- - n_+), \qquad \boldsymbol{E} = -\nabla_{\boldsymbol{R}} \Phi, \tag{4}$$

where charged particles are present only in a bounded region, and the electric field far away from the ionized region is homogeneous. Here n_e, n_+ and n_- are the particle densities of electrons, positive and negative ions, and $\boldsymbol{E}$ and Φ are the electric field and potential, respectively. The total field $\boldsymbol{E}$ is the sum of the background (Laplacian) field $\boldsymbol{E}_b$ in the absence of space charges and the field generated by the charged particles $\boldsymbol{E}'$. μ_e, D_e and ν_a are the electron mobility and diffusion and the electron attachment rate, respectively. e is the electron charge and ϵ_0 is the dielectricity constant. The impact ionization coefficient α_i is a function of the electric field, as established in various books, and for our numerical calculations, we use the Townsend approximation

$$\alpha_i(|\boldsymbol{E}|) = \alpha_0 \exp(-E_0/|\boldsymbol{E}|), \tag{5}$$

in which α_0 and E_0 are parameters for the effective cross section. They depend on the ratio of background and normal gas density (N and N_0, respectively) as $\alpha_0 \propto (N/N_0)$ and $E_0 \propto (N/N_0)$ [22]. This scaling is equivalent to stating that the reduced electric field $\boldsymbol{E}/N$ is the relevant physical variable for impact ionization processes. The positive and negative ions are considered to be immobile on the timescales investigated in this paper because avalanches and streamers evolve on the time scale of the electrons that are much more mobile due to their much lower mass.

We consider the situation where a tiny ionization seed of the size of one or a few free electrons is placed in free space, i.e. within a gas far from walls, electrodes or other boundaries. If the externally applied field is sufficiently high, it will develop into an electron avalanche that will drift toward the anode. Eventually, the charged particle density in the avalanche will become so large that space charge effects set in and change the externally applied field. As a consequence, the interior of the formed very weak plasma will be weakly screened from the external field while the field at the outer edges is enhanced. Depending on photo-ionization processes, an anode-directed or a double ended streamer then emerges from the avalanche. This evolution from an electron avalanche to a streamer is illustrated in figure 1. Details of our simulations can be found in [23–25]; here we only use them for purposes of illustration.

Figure 1 shows essential features of the solutions that will be substantiated by quantitative analysis in the body of the paper. In the left column, an avalanche can be seen: the electron distribution (upper row) is Gaussian and spherically symmetric. The position of the Gaussian is determined by electron drift in the homogeneous background field, its width by electron diffusion. The ions (second row) are left behind (i.e. further down) and stretched along the temporal trace of the avalanche. The resulting space charge distribution (third row) is essentially a smooth dipole without much structure. This particular picture is actually quite similar to the old drawings of Raether [21]. The electric field (fourth row) is essentially unchanged up to corrections below 1%. The current (lowest row) shows the same Gaussian structure as the electrons; it is dominated by electron drift $\mu_e n_e(\boldsymbol{R}, t)\boldsymbol{E}_b$ in the homogeneous background field $\boldsymbol{E}_b$ with a small diffusional correction. In the right column, a conducting filament is formed, and the streamer stage is reached. Electron and ion distribution show a similar long stretched shape. The space charges approach a layered structure, and the field ahead of the streamer is changed by these space charges by up to 40%.

There is some freedom in defining the transition point from avalanche to streamer. In the body of the paper, we will argue that a maximal field enhancement of 3% ahead of the streamer, i.e.,

$$k = \frac{\max_{\boldsymbol{R}} |\boldsymbol{E}(\boldsymbol{R}, t)| - |\boldsymbol{E}_b|}{|\boldsymbol{E}_b|}, \qquad k = 0.03 \tag{6}$$

is a reasonable measure for the transition. We will see that essentially up to this moment of time the total number of electrons in the avalanche grows exponentially in time, while in the streamer phase, the growth is slower.

1.3. Review of critical field and Raether–Meek criterion

Essentially two criteria have been given in the literature for the emergence of a streamer from a tiny ionization seed, one for the required background field and one for the required space and time of evolution. The first criterion is a necessary lower bound for the background field: the electric field has to be

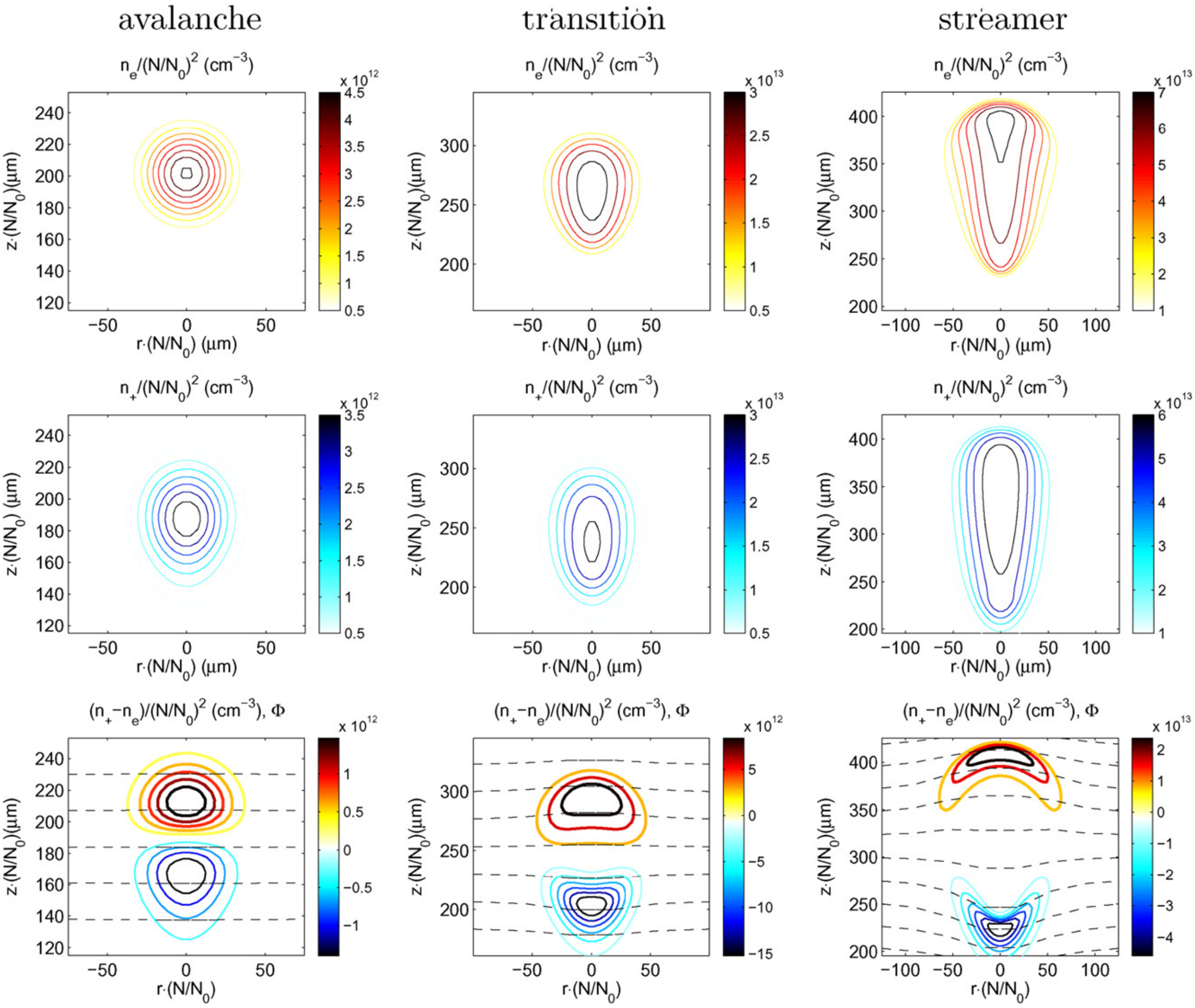

Figure 1. The avalanche to streamer transition: numerical solution of the discharge model (1)–(4) for pure N_2 in a uniform background field. As N_2 is a non-attaching gas, negative ions do not form. The background electric field is directed in the negative z-direction and has a strength $E_b/(N/N_0) = 100\,\mathrm{kV\,cm^{-1}}$, when the parameters from equation (12) are used. Here N is the actual particle density and N_0 the particle density under normal conditions. Initially, a single electron was placed at $z = 115\,\mu$m. Shown are the electron avalanche phase (left column), the transition to streamer (middle column) and the space charge dominated streamer phase (right column). The respective times are $t = 0.225$, 0.375 and 0.525 ns $(N/N_0)^{-1}$ for N_2. From top to bottom (continued on next page): electron number density distribution; ion number density distribution; net charge density distribution (positive: blue thin lines, negative: red thick lines) and equipotential lines (- - - -); electric field strength (smaller than the background field: blue thin lines, larger: red thick lines); current density $\boldsymbol{j}_e = -\mu_e \boldsymbol{E} n_e - D_e \nabla n_e$ (arrows) and level lines of $|\boldsymbol{j}_e|$.

higher than the threshold field E_k where the impact ionization rate overcomes the attachment rate. The ionization level can only grow if the rightmost term in equation (1) is positive, hence if the effective ionization coefficient is positive

$$\alpha(|\boldsymbol{E}|) = \alpha_i(\boldsymbol{E}|) - \nu_a/(\mu_e|\boldsymbol{E}|) > 0. \tag{7}$$

This determines the threshold field E_k as

$$\mu_e\; E_k \alpha_i(E_k) = \nu_a. \tag{8}$$

The second criterion is known as the Raether–Meek criterion. It states that the total electron number must have reached the order of 10^8–10^9 for space charge effects to set in. If this number is reached by exponential multiplication of one initial electron within a constant field $\boldsymbol{E}_b$, this means that

$$\exp\left(\alpha(|\boldsymbol{E}|)d\right) \approx 10^8 \text{ to } 10^9, \tag{9}$$

where d is the avalanche length. In brief as a rule of thumb the criterion reads

$$\alpha(|\boldsymbol{E}|)d \approx 18 \text{ to } 21 \text{ according to Raether and Meek.} \tag{10}$$

Let us first note that the same criterion has been suggested for quite different situations in the literature. In his original article, Meek [26] studies the emergence of a cathode directed (i.e. positive) streamer from an anode directed avalanche that has bridged a short gap. On the other hand, Bazelyan and Raizer [27] study the emergence of streamers in free space, i.e. far away from the electrodes. To estimate the field of the ions, Meek used the diffusion radius of the electron avalanche, and the ionization rate in the background field; however, the diffusion does not show up in his transition criterion. Bazelyan and Raizer on the other hand, neglect diffusion and base their criterion on the radius of the avalanche due to electrostatic

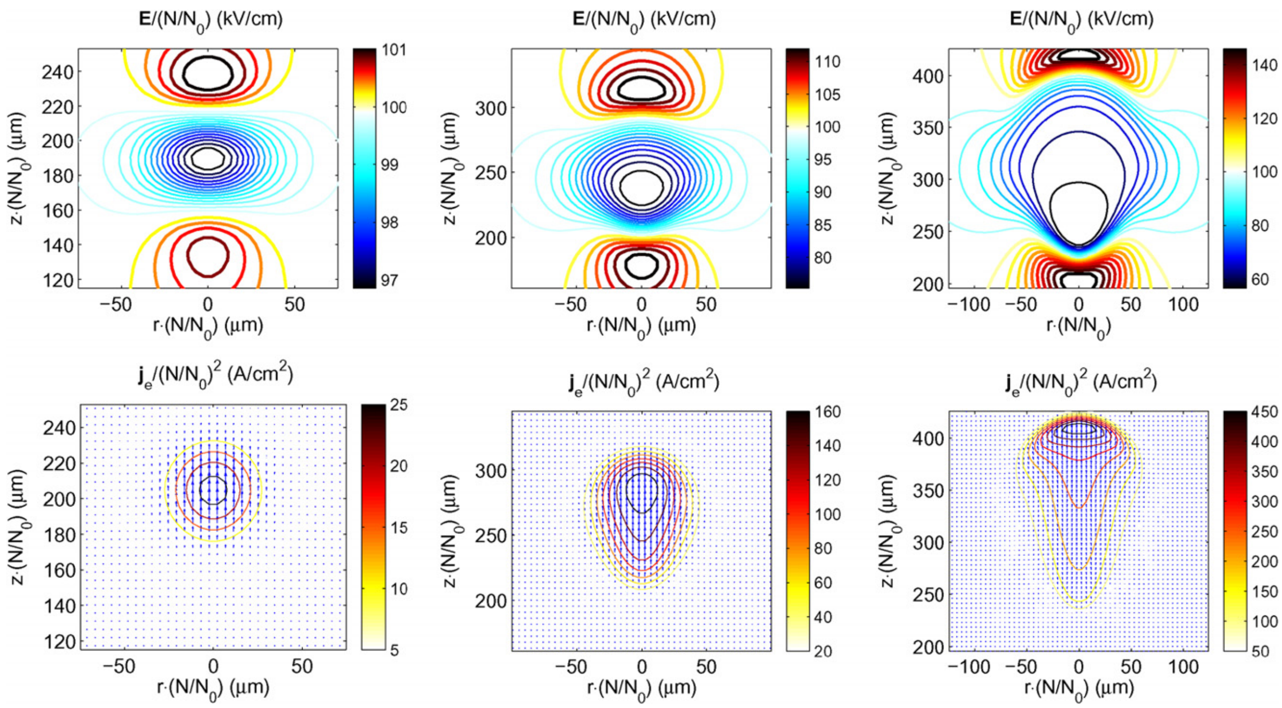

Figure 1. Continued.

repulsion. All authors [26–29] assume the electron distribution to be spherically symmetric; on the other hand, they base their transition criterion on a total field screening, i.e. on $k = 1$ in equation (6). In view of available simulation results like our figure 1, these assumptions are clearly inconsistent.

Apart from these considerations of the history of the derivation, there are actually two major reasons to revise the Raether–Meek-criterion which are the following.

(1) The prediction that a parameter should be in the range of 18–21 (where authors seem to be willing to assume an even larger range of values to get consistency with the experiment) is not very satisfactory and invites improvement.
(2) Diffusion has to be included into the model for physical as well as for mathematical reasons. Without diffusion, an initially concentrated electron package would not spread and it would create enormous fields within a very short time as they are well known in the neighbourhood of point sources. Indeed, diffusion decreases the electron density and the maximal fields while impact ionization increases it. In low fields, diffusion stays dominant for a long time and delays space charge effects and consecutive streamer emergence. It is therefore clear that the avalanche to streamer transition does not only depend on multiplication rates, but also on the relative importance of diffusional spreading. This should provide a more quantitative transition criterion than the pure Raether–Meek criterion.

1.4. Organization of the paper

We will derive a diffusion correction to the Raether–Meek criterion through the following steps: in section 2, the intrinsic scales of the problem with their explicit density dependence are identified through dimensional analysis. In section 3, we analyse the spatial distribution of the electrons during the avalanche phase and their contribution to the electric field; this gives a first approximate correction to the Raether–Meek-criterion. In section 4, we approximate the spatial distribution of the ions and their contribution to the electric field. Electron and ion field are then combined to give the total change of the electric field during the avalanche phase. If this field becomes 'substantial' (cf figure 1 and equation (6)), we have found the avalanche-to-streamer transition. Finally, the analytical non-dimensional results are translated back to dimensional quantities, and we refer the reader interested in the final prediction only to figures 5 and 6 for the transition criterion in non-attaching gases and in air. These figures visualize the analytical criterion (53) or (54). Section 5 contains the conclusions. Appendix A summarizes the parameter values used for air, and appendix B contains an approximation for the electric field generated by the ion cloud that differs from the one presented in section 4.

2. Dimensional analysis

The Raether–Meek criterion can be understood as a simple example of dimensional analysis. Dimensional analysis identifies general physical properties in terms of dimensionless numbers that are independent of a particular gas type or density. The physical importance of dimensionless numbers like the Reynolds number is well known in hydrodynamics; we follow the same approach here.

In the light of dimensional analysis, the Raether–Meek criterion states that the effective cross-section $\alpha(|\boldsymbol{E}|)$ has the dimension of inverse length, hence the dimensionless number $\alpha(|\boldsymbol{E}|)d$ characterizes the gap length in multiples of the ionization length and therefore the exponential multiplication rate $e^{\alpha d}$. This number directly gives the total number of electrons in an avalanche after a travel distance d if the avalanche started with a single free electron. However, this is not the only dimensionless number in the problem, a second one is the dimensionless diffusion constant

$$D = \frac{D_e \alpha_0}{\mu_e E_0}, \tag{11}$$

that plays a distinctive role in the avalanche to streamer transition as it determines the width of the electron cloud. Note that this dimensionless diffusion constant is related to the electron temperature as $D_e/\mu_e = k_B T_e$ where k_B is the Boltzmann constant. The electron temperature T_e actually can be defined through this relation, even if the electron energy distribution is not Maxwellian in the presence of strong electric fields. Furthermore, D depends on α_0/E_0, where the parameters α_0 and E_0 characterize the impact ionization reaction (5) for a specific gas type and density. We remark that the impact ionization reaction need not have the Townsend form for this analysis.

For the setup of dimensional analysis, we refer to earlier papers [30, 31] and only state the results here: lengths are measured in units of $\ell_0 = 1/\alpha_0$, electric fields in units of E_0, velocities in units of $v_0 = \mu_e E_0$ and time consistently in units of $t_0 = 1/(\alpha_0 \mu_e E_0)$—hence diffusion should be measured in units of $v_0 \ell_0 = \mu_e E_0/\alpha_0$ as done in (11). The natural scale for the particle densities follows from the Poisson equation, $n_0 = \epsilon_0 \alpha_0 E_0/e$.

The parameters α_0, μ_e, D_e and E_0 depend on the ratio of the background gas density N and the gas density under normal conditions N_0. For instance, using parameters as in [22,32–34], the characteristic scales for N_2 are

$$\begin{aligned}
&\ell_0 = \frac{1}{\alpha_0} = 2.3\ \mu\text{m}\ \frac{1}{N/N_0}, && E_0 = 200\text{kV cm}^{-1}\frac{N}{N_0},\\
&\mu_e = 380\ \text{cm}^2\ (\text{V s})^{-1}\frac{1}{N/N_0}, && D_e = 1800\ \text{cm}^2\ \text{s}^{-1}\frac{1}{N/N_0},\\
&v_0 = \mu_e E_0 = 7\cdot 10^7\ \text{cm s}^{-1}, && t_0 = \frac{\ell_0}{v_0} = 3\ \text{ps}\frac{1}{N/N_0},\\
&n_0 = \frac{\epsilon_0\alpha_0 E_0}{\text{e}} = \frac{4.8\cdot 10^{14}}{\text{cm}^3}\left(\frac{N}{N_0}\right)^2, && D = \frac{D_e}{v_0\ell_0} = 0.1.
\end{aligned} \tag{12}$$

Note that the characteristic velocity scale is independent of gas density, in rough agreement with measurements of streamer velocities at different pressures. Note furthermore, that this analysis directly shows that the relevant physical parameter is the reduced electric field $\boldsymbol{E}/N$.

Dimensionless parameters and fields are introduced as

$$\begin{aligned}
&\boldsymbol{r} = \frac{\boldsymbol{R}}{\ell_0}, && \tau = \frac{t}{t_0}, && \nu = \nu_a t_0,\\
&\sigma = \frac{n_e}{n_0}, && \rho = \frac{n_+ - n_-}{n_0}, && \boldsymbol{\mathcal{E}} = \frac{\boldsymbol{E}}{E_0},
\end{aligned} \tag{13}$$

which brings the system of equations (1)–(4) into the dimensionless form

$$\partial_\tau \sigma = D\nabla^2\sigma + \nabla(\boldsymbol{\mathcal{E}}\sigma) + f(|\boldsymbol{\mathcal{E}}|, \nu)\sigma, \tag{14}$$

$$\partial_\tau \rho = f(|\boldsymbol{\mathcal{E}}|, \nu)\sigma, \tag{15}$$

$$-\nabla^2\phi = \rho - \sigma \qquad \boldsymbol{\mathcal{E}} = -\nabla\phi, \tag{16}$$

where the operator ∇ is taken with respect to $\boldsymbol{r}$ and where $f(|\boldsymbol{\mathcal{E}}|, \nu)$ is the dimensionless effective ionization rate,

$$f(|\boldsymbol{\mathcal{E}}|, \nu) = \frac{\mu_e|\boldsymbol{E}|\alpha_i(|\boldsymbol{E}|) - \nu_a}{\mu_e E_0 \alpha_0} = |\boldsymbol{\mathcal{E}}|\text{e}^{-1/|\boldsymbol{\mathcal{E}}|} - \nu. \tag{17}$$

It is remarkable that the density of positive and negative ions $n_\pm$ enters the equations only in the form of the single dimensionless field $\rho \propto n_+ - n_-$. This is clear in the case of the Poisson equation, but holds also for the generation term proportional to $f(|\boldsymbol{\mathcal{E}}|, \nu)$. This coefficient accounts for the production of free electrons and positive ions through impact ionization and for the loss of free electrons and generation of negative ions due to attachment.

We neglect the effect of photoionization as its rates are typically much lower than impact ionization rates; it does not contribute significantly to the build-up of a compact ionized cloud where eventually space charge effects will set in (quite in contrast to its distinct role in positive streamer propagation).

3. Electron distribution and field

We derive the transition as follows: we assume that an avalanche starts from a single electron and follows a transition as shown in figure 1. In the calculation we neglect space charge effects on the evolution of densities, but we do calculate the additional electric field generated by the space charges. If this field reaches a relative value of k = 0.03—this value will be motivated in section 4.4—space charge effects are not negligible anymore, and the transition to the streamer is found.

The electric field generated by space charges has one contribution from the electrons σ and another one from the positive and negative ions ρ. In the present section, we calculate the field of the electrons; in the next section, we will include the field of the ions.

3.1. The electron distribution: a Gaussian

We write the single electron that generates the avalanche as a localized initial density

$$\sigma(\boldsymbol{r}, \tau = 0) = \rho(\boldsymbol{r}, \tau = 0) = \sigma_0\delta(\boldsymbol{r} - \boldsymbol{r}_0) \tag{18}$$

and consider its evolution under the influence of a uniform field $\boldsymbol{\mathcal{E}}_b = -\mathcal{E}_b\hat{\boldsymbol{e}}_z$, where $\hat{\boldsymbol{e}}_z$ is the unit vector in the z direction and $\mathcal{E}_b = |\boldsymbol{\mathcal{E}}_b|$ is constant. A single electron is written as a δ-function $n_e(\boldsymbol{R}) \propto \delta^3(\boldsymbol{R} - \boldsymbol{R}_0)$ in physical units where the spatial integral over the electron number density

$$N_e(\tau) = \int d^3\boldsymbol{R}\ n_e(\boldsymbol{R}), \tag{19}$$

of course, should be unity at time $\tau = 0$: $N_e(0) = 1$. According to the last section, this corresponds in dimensionless units to

$$\sigma_0 = \frac{1}{n_0\ell_0^3}, \tag{20}$$

which is $1.7\cdot 10^{-4}\ N/N_0$ for nitrogen. We will use $\sigma_0 = 10^{-4}$ in what follows. We emphasize, however, that the theory will be developed for an arbitrary value of σ_0.

During the avalanche phase the electric field remains unaffected by space charges, so that the continuity equations for the charged particles (14)–(15) can be linearized around the background field,

$$\partial_\tau \sigma = D\nabla^2\sigma + \boldsymbol{\mathcal{E}}_b \cdot \nabla\sigma + \sigma f, \tag{21}$$

$$\partial_\tau \rho = \sigma f, \tag{22}$$

where $f = f(\mathcal{E}_b, \nu)$.

For the initial condition (18), the electron evolution according to equation (21) can be given explicitly as [22]

$$\sigma(\boldsymbol{r}, \tau) = \sigma_0\, \mathrm{e}^{f(\mathcal{E}_b,\nu)\tau} \frac{\exp[-(\boldsymbol{r} - \boldsymbol{r}_0 + \boldsymbol{\mathcal{E}}_b\tau)^2/(4D\tau)]}{(4\pi D\tau)^{3/2}}; \tag{23}$$

it has the form of a Gaussian package that drifts with velocity $-\boldsymbol{\mathcal{E}}_b$, widens diffusively with half width proportional to $\sqrt{4D\tau}$ and carries a total number of electrons $\sigma_0 \mathrm{e}^{f(\mathcal{E}_b,\nu)\tau}$. (If the initial ionization seed consists of several electrons in some close neighbourhood, the Gaussian shape is approached nevertheless for large times due to the central limit theorem.)

Integrating equation (23) over the entire space shows that the total number of electrons at time τ is $N_e(\tau) = \sigma_0 n_0 \ell_0^3 \mathrm{e}^{f\tau}$. On the other hand, the maximum of the electron density is reached at the centre of the Gaussian $\boldsymbol{r} = \boldsymbol{r}_0 - \boldsymbol{\mathcal{E}}_b\tau$ and has the value

$$\sigma_{\max}(\tau) = \max_{\boldsymbol{r}} \sigma(\boldsymbol{r}, \tau) = \frac{\sigma_0\, \mathrm{e}^{f\tau}}{(4\pi D\tau)^{3/2}}, \tag{24}$$

hence it first decreases until $\tau = 3/(2f)$ due to diffusion and then increases due to electron multiplication. At this moment of evolution, generation overcomes diffusion.

The axial electron density distribution for a background field of $\boldsymbol{\mathcal{E}}_b = 0.25$ at $\tau = 2000$ (for N_2 this corresponds to a reduced electric field $E_b(N_0/N) = 50\,\mathrm{kV\,cm^{-1}}$ and $t = 6\,\mathrm{ns}$) is illustrated in the upper panel of figure 2. Here the analytical solution (23) of the linearized continuity equation (21) is compared with a numerical evaluation of the full nonlinear problem (14)–(16). The excellent correspondence between the solution of both the linearized and the nonlinear problem shows that, at this time, space charge effects are negligible, so that the discharge is still in the avalanche phase.

3.2. Exact result for the electron generated field $\mathcal{E}_\sigma$

While the density and field of the ions can only be calculated approximately and will be treated in the next section, the electric field $\boldsymbol{\mathcal{E}}_\sigma$ generated by the Gaussian electron package can be calculated exactly.

The main point is that the electron density distribution (23) is spherically symmetric about the point $\boldsymbol{r}_0 - \boldsymbol{\mathcal{E}}_b\tau$. The electric field $\boldsymbol{\mathcal{E}}_\sigma(s, \tau)$ at the point

$$\boldsymbol{s} = \boldsymbol{r} - \boldsymbol{r}_0 + \boldsymbol{\mathcal{E}}_b\tau \tag{25}$$

can therefore be written as $\boldsymbol{\mathcal{E}}_\sigma(s, \tau) = -\mathcal{E}_\sigma(s, \tau)\hat{\boldsymbol{e}}_s$, where $\hat{\boldsymbol{e}}_s$ is the unit vector in the radial $\boldsymbol{s}$ direction. Its magnitude can be computed with Gauss' law of electrostatics (in the same way as the gravitational force field of a spherically symmetric mass distribution). It uses the fact that the field at radius s is determined by the total charge inside the sphere of radius s, and it is independent of charges outside this radius, as long as the distribution is spherically symmetric. The calculation yields

$$\mathcal{E}_\sigma(s, \tau) = \frac{1}{s^2}\int_0^s \sigma_0 \mathrm{e}^{f\tau} \frac{\mathrm{e}^{-r^2/(4D\tau)}}{(4\pi D\tau)^{3/2}} r^2 \mathrm{d}r = \frac{\sigma_0 \mathrm{e}^{f\tau}}{16\pi D\tau} F\left(\frac{s}{\sqrt{4D\tau}}\right), \tag{26}$$

with

$$F(x) = \frac{1}{x^2}\frac{4}{\sqrt{\pi}}\int_0^x y^2 \mathrm{e}^{-y^2}\mathrm{d}y = \frac{\mathrm{erf}\,x}{x^2} - \frac{2}{\sqrt{\pi}}\frac{\mathrm{e}^{-x^2}}{x} = \begin{cases} \dfrac{4}{3\sqrt{\pi}}x & \text{for } x \ll 1 \\ \dfrac{1}{x^2} & \text{for } x \gg 1, \end{cases} \tag{27}$$

where erf is the error function. Far outside the electron cloud at $x \gg 1$, this expression reproduces the $1/x^2$ decay of the electric field, while inside the cloud for $x \ll 1$, the field increases like x.

The spatial maximum of the field strength $\mathcal{E}_\sigma$ is determined by the maximum of $F(x)$; evaluating $\mathrm{d}_x F(x) = 0$ shows that it is located at an x such that

$$\frac{2}{\sqrt{\pi}}(x + x^3)\mathrm{e}^{-x^2} = \mathrm{erf}\; x. \tag{28}$$

Solving this equation numerically leads to a position of the maximum of $x \simeq 1$ (which is the radius at which the Gaussian electron distribution has dropped to $1/e$ of its maximal value) and to the value $F(1) \simeq 0.4276$. Hence, the spatial maximum of the electron generated electric field strength becomes

$$\mathcal{E}_\sigma^{\max}(\tau) \simeq \frac{\sigma_0 \mathrm{e}^{f\tau}}{16\pi D\tau} F(1), \tag{29}$$

it is located on the sphere parameterized through

$$|\boldsymbol{r} - \boldsymbol{r}_0 - \boldsymbol{\mathcal{E}}_b\tau| \simeq \sqrt{4D\tau}. \tag{30}$$

In the original cylindrically symmetric coordinate system (r, z), the axial field component is directed in the negative z-direction, i.e. in the same direction as the background field, 'ahead' of the electron cloud ($z > z_0 + \mathcal{E}_b\tau$) as illustrated by the solid line in the lower panel of figure 2. Together with equation (30), we find that the maximal field strength $|\boldsymbol{\mathcal{E}}_b + \boldsymbol{\mathcal{E}}_\sigma|$ and its location are

$$\max_{\boldsymbol{r}} |\boldsymbol{\mathcal{E}}_b + \boldsymbol{\mathcal{E}}_\sigma| = |\boldsymbol{\mathcal{E}}_b + \boldsymbol{\mathcal{E}}_\sigma|(\boldsymbol{r}_m, \tau) = \mathcal{E}_b + \mathcal{E}_\sigma^{\max}(\tau), \tag{31}$$

$$\boldsymbol{r}_m(\tau) \simeq (z_0 + \mathcal{E}_b\tau + \sqrt{4D\tau})\hat{\boldsymbol{e}}_z. \tag{32}$$

3.3. A lower bound for the transition

Since the avalanche to streamer transition takes place when space charge effects start to affect the electric field, we choose to base the criterion for the transition on the maximal relative field enhancement $k(\tau)$ defined in equation (6), which for the dimensionless field simply reads

$$k(\tau) = \frac{\max_{\boldsymbol{r}} |\boldsymbol{\mathcal{E}}(\boldsymbol{r}, \tau)| - |\boldsymbol{\mathcal{E}}_b|}{|\boldsymbol{\mathcal{E}}_b|}. \tag{33}$$

Here $\boldsymbol{\mathcal{E}} = \boldsymbol{\mathcal{E}}_b + \boldsymbol{\mathcal{E}}_\sigma + \boldsymbol{\mathcal{E}}_\rho$ is the total electric field, and $\boldsymbol{\mathcal{E}}_\sigma$ and $\boldsymbol{\mathcal{E}}_\rho$ are the fields generated by the electrons and the ions,

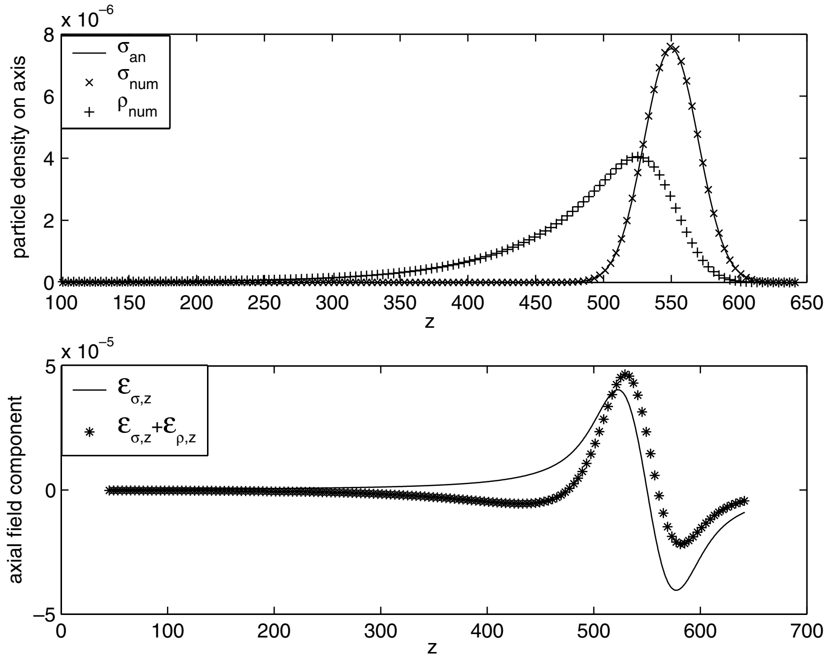

Figure 2. Particle densities (upper panel) and electric fields (lower panel) on the axis ($r = 0$) of the discharge in a background field of $\mathcal{E}_b = -0.25\,\hat{\boldsymbol{e}}_z$, with parameter values for pure N_2: $D = 0.1$, $\nu = 0$ and $\sigma_0 = 10^{-4}$. The initial condition is located at $\boldsymbol{r}_0 = 50\,\hat{\boldsymbol{e}}_z$. The time of the snapshot is $\tau = 2000$. This stage corresponds qualitatively to the leftmost column of figure 1. Upper panel: electron (x) and ion (+) density distributions computed numerically for the full nonlinear model (14)–(16); the solid line is the analytical solution (23) for the electron density distribution neglecting space charge effects. Numerical solution and analytical approximation coincide perfectly. Lower panel: numerical solution of the electric field generated by the full space charge distribution of electrons and ions $\boldsymbol{\mathcal{E}}' = \boldsymbol{\mathcal{E}}_\sigma + \boldsymbol{\mathcal{E}}_\rho = \boldsymbol{\mathcal{E}} - \boldsymbol{\mathcal{E}}_b$ ($*$) and the analytical result (27) for the field $\boldsymbol{\mathcal{E}}_\sigma$ generated by the electrons only (——). Analytical approximations for the field generated by the ions $\boldsymbol{\mathcal{E}}_\rho$ will be discussed in the next section.

respectively. We will show in the next section that $k_t = 0.03$ is an appropriate estimate for the maximal relative field enhancement at the mid gap avalanche to streamer transition. At lower values of k, space charge effects can be neglected, whereas at higher values the dynamics of the electrons are nonlinear and the full streamer equations (14)–(16) have to be solved.

As a first estimate for the space charge field, and thereby for the avalanche to streamer transition, we compute the field generated by the electrons only and neglect the ion field. This is a reasonable approximation, as the lower panel in figure 2 shows. Actually, the magnitude of the monopole field $\boldsymbol{\mathcal{E}}_\sigma$ ahead of the electron cloud is an upper bound for the magnitude of the field created by the dipole of electrons on the one hand and the positive charges left behind by the electron cloud on the other. Therefore, the maximal relative field enhancement due to the electrons, $k_\sigma(\tau) = \mathcal{E}_\sigma^{max}(\tau)/\mathcal{E}_b$, exceeds the transition value after a shorter travel time τ_σ and distance than the genuine relative field enhancement $k(\tau)$ of equation (33). Hence, τ_σ is a lower bound for the time of the avalanche-to-streamer transition.

This lower bound τ_σ for the transition can be expressed through equation (29) as

$$f\tau_\sigma - \ln(\mathcal{E}_b\tau_\sigma) \simeq \ln\frac{16\pi k_t D}{F(1)\sigma_0}. \tag{34}$$

As travel time and travel distance are related through the drift velocity $\mathcal{E}_b$, the value $f(|\boldsymbol{\mathcal{E}}_b|, \nu)\tau_\sigma$ is found to be identical to $(\alpha(E_b) - \nu_a/\mu_e E_b)d_\sigma$ in dimensional units where

$$d_\sigma = v_0 t_\sigma = \mu_e E_b t_\sigma \tag{35}$$

is the avalanche travel distance. In dimensional quantities, using the Townsend scales α_0 and E_0 and the initial condition $\sigma_0 = 10^{-4}\,N/N_0$, equation (34) takes the form

$$\left(\alpha_i(E_b) - \frac{\nu_a}{\mu_e E_b}\right)d_\sigma - \ln(d_\sigma\alpha_0) = \ln\frac{16\pi k_t}{F(1)10^{-4}} + \ln\frac{D_e\alpha_0}{\mu_e E_0} - \ln\frac{N}{N_0}. \tag{36}$$

For a non-attaching gas ($\nu_a = 0$) at atmospheric pressure under normal conditions with dimensionless diffusion comparable to nitrogen, inserting the numerical values for the parameters, we obtain

$$\alpha(E_b)d_\sigma - \ln(\alpha_0 d_\sigma) \approx 9.4. \tag{37}$$

f being a growing function of $|\boldsymbol{\mathcal{E}}_b|$, equation (34) shows that the larger the field, the earlier the transition takes place, which is in accordance with Meek's criterion. On the other hand, the second term on the right-hand side of equation (36) depends on the diffusion coefficient in such a way that diffusion delays the transition to streamer, as expected.

The solution $\alpha(E_b)d_\sigma$ for N_2 at atmospheric pressure is shown in the dash–dotted line of figure 3, where it is compared with a numerical evaluation of the transition time (circles). The latter data have been obtained through a full simulation of the continuity equations (14) and (15) together with the Poisson equation (16) [31, 23] that was also used to generate figure 1. Though the qualitative features of the transition time are well reproduced, this figure shows that the underestimation of the transition time is significant and that it is necessary to include the field of the ion trail left behind by the electrons.

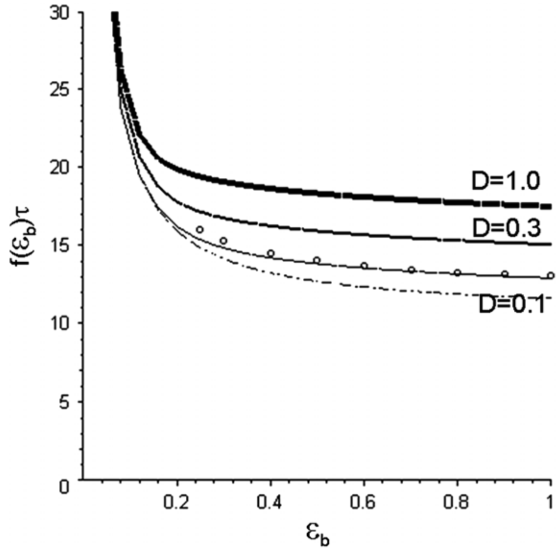

Figure 3. The dimensionless transition time $f\tau$ (equivalent to the dimensional travel distance αd) as a function of the background electric field for $\sigma_0 = 10^{-4}$, $\nu = 0$ and different values of D. Solid lines are computed with equation (53) for $D = 0.1$ (——), 0.3 (medium thin line) and 1 (thickest line); dash-dotted lines are computed with equation (34) for $D = 0.1$; symbols denote full numerical evaluation for $D = 0.1$. Obviously, the approximation (53) fits the full numerical results very well.

4. Ion distribution and field

4.1. Exact results on the spatial moments of the distributions

To get a more accurate estimate for the avalanche-to-streamer transition, the field generated by the positive and negative ions has to be included. In the case of the ion distribution, closed analytical results cannot be found, in contrast to the case of the electron distribution (23). However, arbitrary spatial moments of the distribution

$$\langle \mathcal{O}\rangle_\rho = \frac{\int \mathcal{O}\rho d^3\boldsymbol{r}}{\int \rho d^3\boldsymbol{r}}, \qquad \text{where } \mathcal{O} = z^n \text{ or } r^n, \tag{38}$$

can be derived analytically. Here z is the direction of the homogeneous field $\mathcal{E}_b$ and r is the radial direction. First, the evolution equation (15) for the ion density ρ is integrated in time and the analytical form (23) for $\sigma(\boldsymbol{r},\tau)$ is inserted. As $f = f(|\boldsymbol{\mathcal{E}}_b|,\nu)$ is constant in space and time one finds

$$\rho(\boldsymbol{r},\tau) - \rho(\boldsymbol{r},0) = f\sigma_0\int_0^\tau d\tau' \mathrm{e}^{f\tau'}\,\frac{\exp\left[-(z-z_0-\mathcal{E}_b\tau')^2/(4D\tau')\right]}{\sqrt{4\pi D\tau'}} \times\frac{\exp\left[-r^2/(4D\tau')\right]}{4\pi D\tau'}. \tag{39}$$

Here the initial perturbation is located at z_0 on the axis $r = 0$. The moments (38) can now be derived from (39) by exchanging the order of spatial and temporal integration. In particular, one finds

$$\int \rho d^3\boldsymbol{r} = \sigma_0 e^{f\tau},$$

$$\int z\rho d^3\boldsymbol{r} = \sigma_0 e^{f\tau}\left(z_0 + \mathcal{E}_b\tau - \frac{1-e^{-f\tau}}{f/\mathcal{E}_b}\right), \tag{40}$$

and higher moments can be calculated in the same way. For the moments of ρ in the axial direction, this gives

$$\langle z\rangle_\rho = z_0 + \mathcal{E}_b\left(\tau - \frac{1}{f}\right) + O(\mathrm{e}^{-f\tau}), \tag{41}$$

$$\langle z^2\rangle_\rho - \langle z\rangle_\rho^2 = \left(\frac{\mathcal{E}_b}{f}\right)^2 + 2D\left(\tau - \frac{1}{f}\right) + O(\mathrm{e}^{-f\tau}). \tag{42}$$

The second moment of ρ in the radial direction is

$$\langle r^2\rangle_\rho = 2D\left(\tau - \frac{1}{f}\right) + O(\mathrm{e}^{-f\tau}). \tag{43}$$

For comparison, the moments of the Gaussian electron distribution (23) are easily found to be

$$\langle z\rangle_\sigma = z_0 + \mathcal{E}_b\tau, \tag{44}$$

$$\langle z^2\rangle_\sigma - \langle z\rangle_\sigma^2 = 2D\tau, \tag{45}$$

$$\langle r^2\rangle_\sigma = 2D\tau. \tag{46}$$

4.2. Discussion of the moments

Let us now interpret these moments. A first moment of a spatial distribution gives the position of its centre of mass. For the second moment, the cumulant

$$\langle z^2\rangle_x^c := \langle (z - \langle z\rangle_x)^2\rangle_x = \langle z^2\rangle_x - \langle z\rangle_x^2, \qquad x = \sigma, \rho. \tag{47}$$

measures the quadratic extension from the centre of mass. As the centre of mass lies on the axis, for the radial extension the distinction between second moment and its cumulant need not be made.

The moments for the electrons (44)–(46) have a simple structure: the centre of mass of the electron package is located at $z = z_0 + \mathcal{E}_b\tau$, and the package has a diffusive width $\sqrt{2D\tau}$ around it, both in the forward z direction and in the radial r direction.

The ion cloud shows a more complex behaviour; it is evaluated close to the avalanche-to-streamer transition where $f\tau = \alpha d = O(10)$, therefore the terms of order $\mathrm{e}^{-f\tau}$ are neglected.

First it is remarkable that the centre of mass of the ion cloud (41) moves with precisely the same velocity as the electron cloud though the ion motion is neglected while the electrons drift. Therefore the ion cloud "motion" is purely due to the generation of additional ions at the front part of the cloud. As a consequence, the centre of mass of the ion cloud is at an approximately constant distance $\mathcal{E}_b/f$ behind the electron centre of mass. This dimensionless distance

$$\ell_\alpha = \frac{\mathcal{E}_b}{f(\mathcal{E}_b)} = \frac{\alpha_0}{\alpha(E_b)} \tag{48}$$

corresponds to the dimensional ionization length $1/\alpha(E_b)$.

The quadratic radial width of the ion cloud $2D(\tau - 1/f)$ is $2D/f$ smaller than that of the electron cloud. This is related to the fact that the electron cloud also was more narrow at the earlier time when it left the ions behind. The ion cloud is more extended in the z direction. More precisely, its length is ℓ_α larger than its width. This is because the ions are immobile, therefore a trace of ions is left behind by the electron cloud.

Moreover, it can be remarked that the difference between quadratic width and length of the ion cloud is given by the same ionization length ℓ_α as the distance between the centres of mass of the ion and the electron cloud. We refer to the left column of figure 1 for the illustration of these density distributions.

4.3. An estimate for the transition

One can assume as in [27] that the ions have a spatial distribution similar to the electrons, thus a Gaussian with the same width as the electron cloud, but centred around $r = 0$ and $z = \langle z\rangle_\rho$:

$$\rho_1(r, z, \tau) = \sigma_0\, \mathrm{e}^{f\tau} \frac{\exp\left[-[(z - \langle z\rangle_\rho)^2 + r^2]/(4D\tau)\right]}{(4\pi D\tau)^{3/2}}. \qquad (49)$$

In this approximation, the total electric field becomes

$$\boldsymbol{\mathcal{E}}_1(r, z, \tau) = \boldsymbol{\mathcal{E}}_b - \frac{\sigma_0 \mathrm{e}^{f t}}{16\pi\ D\tau}\left[F\left(\frac{|\boldsymbol{s}_\sigma|}{\sqrt{4D\tau}}\right)\frac{\boldsymbol{s}_\sigma}{|\boldsymbol{s}_\sigma|} + F\left(\frac{|\boldsymbol{s}_\rho|}{\sqrt{4D\tau}}\right)\frac{\boldsymbol{s}_\rho}{|\boldsymbol{s}_\rho|}\right], \qquad (50)$$

where

$$\boldsymbol{s}_x = \boldsymbol{r} - \langle z\rangle_x \hat{\boldsymbol{e}}_z \text{ for } x = \rho, \sigma \qquad (51)$$

are the distances to the electron and ion centres of mass and $F(x)$ was defined in equation (27).

The maximum of the field $\mathcal{E}_1$ cannot be computed analytically. However, in figure 1 and in the lower panel of figure 2, it can be seen that this maximum is located on the axis ahead of the electron cloud and that the location of the maximum of the total field and that of the electron field nearly coincide. This can easily be explained physically: the total field is the sum of the fields induced by the electrons and by the ions. Its maximum is located just ahead of the electron cloud, where the electron field is large and varies rapidly, while the field contribution of the ions is smoother and smaller since the observation point is further away from the ion cloud. Therefore the maximum position of the total field is essentially identical to the maximum position of the electron field. This justifies our approximation to evaluate the field $\mathcal{E}_1$ at the maximum position $\boldsymbol{r}_m$ of $|\boldsymbol{\mathcal{E}}_b + \boldsymbol{\mathcal{E}}_\sigma|$ as defined in equation (32). The maximum of the electric field can thus be approximated as

$$\mathcal{E}_1^{\max}(\tau) \simeq \mathcal{E}_1(r = 0, z = z_0 + \boldsymbol{\mathcal{E}}_b\tau + \sqrt{4D\tau}, \tau) = \mathcal{E}_b + \frac{\sigma_0 \mathrm{e}^{f\tau}}{16\pi D\tau}\left[F(1) - F\left(1 + \sqrt{\frac{\ell_\alpha^2}{4D\tau}}\right)\right], \qquad (52)$$

where we recall that the maximum of $F(x)$ lies at $x \approx 1$. Then $\mathcal{E}_1^{max} - \mathcal{E}_b = k\mathcal{E}_b$ implies for the transition time τ_1,

$$f\tau_1 - \ln(\mathcal{E}_b\tau_1) + \ln \frac{F(1) - F\left(1 + \sqrt{\frac{\ell_\alpha^2}{4D\tau_1}}\right)}{F(1)} = \ln \frac{16\pi k D}{F(1)\sigma_0}. \qquad (53)$$

The additional term compared with (34) is the third term on the left-hand side of equation (53); the argument of this logarithm is smaller than 1, therefore criterion (53) gives a later transition time and therefore larger travel distance than equation (34) that was based on the field of the electrons only. This is what we expect since the ions tend to reduce the field generated by the electrons ahead of the avalanche and thus the effect of space charge, cf the lower panel in figure 2. The correction given by the ion field is a function of the ratio of the ionization length ℓ_α and the diffusion length $\sqrt{2D\tau}$. At early times, this ratio diverges and $F(\infty) = 0$; at this stage the correction due to the ion cloud is negligible. However, at later times, the correction becomes significant. All these statements are an interpretation of equation (53).

Finally, we translate the criterion back to dimensional units. In section 4, we did so assuming the Townsend form (5) for the ionization coefficient and scaling with gas density; here we assume for a change a more general dependence, where the mobility and diffusion constant can depend on the electric field. Then we find

$$\alpha d - \ln(\alpha d) + \ln\left(F(1) - F\left(1 + \sqrt{\frac{\mu_e(E_b)}{D_e(E_b)}\frac{E_b}{\alpha}\frac{1}{4\alpha d}}\right)\right) = 0.41 - \ln\left(\frac{\mu_e(E_b)}{D_e(E_b)}\frac{\mathrm{e}}{\epsilon_0}\right),$$

where

$$\alpha = \alpha(E_b) = \alpha_i(E_b) - \frac{\nu_a}{\mu_e(E_b)\, E_b}, \qquad (54)$$

and where the transition number $k = 0.03$ was inserted. We recall that $F(x)$ was defined in equation (27) and has its maximum at $x \approx 1$. Equation (54) determines the travel distance d for the avalanche-to-streamer transition when the discharge starts from a single electron.

4.4. The analytically approximated transition criterion compared with numerical results

We now compare again our analytical results for the linearized problem to the outcome of numerical simulations of the full nonlinear model (14)–(16).

In the upper panel of figure 4 the evolution of the maximal electron density as a function of $f(|\boldsymbol{\mathcal{E}}_b|)\tau$ is shown. Numerical and analytical solutions coincide during the avalanche phase, but deviate eventually. This enables us to estimate the moment at which the space charge effects set in, and thus, when the streamer regime is reached. In the lower panel of figure 4 the evolution of the maximal relative field enhancement is considered. Looking at the simulation results (the solid lines), we see that $k = 0.03$ gives a good estimate of the transition time.

The approximation (52) for the maximal field is much better than the previous approximation (29) based on the electron cloud only. Indeed, for example in the case of $\mathcal{E}_b = 0.5$ (corresponding to the medium thick lines), the numerically computed field (solid line) reaches the transition value $|\boldsymbol{\mathcal{E}}_{\mathrm{num}} - \boldsymbol{\mathcal{E}}_b| = 0.03|\boldsymbol{\mathcal{E}}_b|$ at $f\tau \approx 14$. When only the field of the electrons is taken into account, this value would already be reached at $f\tau \approx 12.6$, while the correction based on the approximation of the ion cloud leads to a transition time of $f\tau \approx 13.9$. The correction becomes especially important at higher fields. In low fields, the approximation of the ion distribution and field shows somewhat larger deviations. We note that the analytical approximation ρ_1 is narrower and higher than the genuine one, and therefore leads to an overestimation of the field generated by the ions inside the

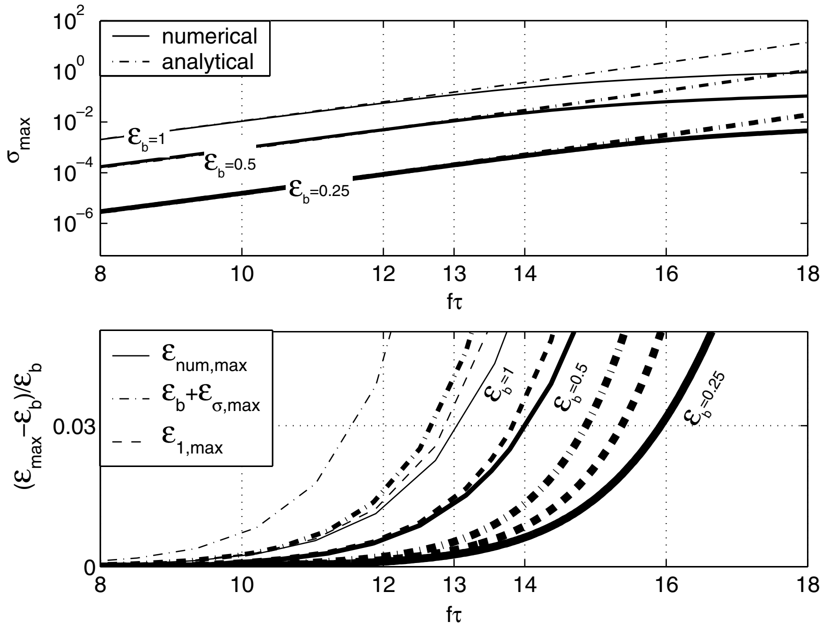

Figure 4. Comparison of analytical approximations and simulation results of the full nonlinear streamer equations (14)–(16) for various background electric field strengths $\mathcal{E}_b$. Thin lines: $\mathcal{E}_b = 1$, medium thick lines: $\mathcal{E}_b = 0.5$ and thick lines: $\mathcal{E}_b = 0.25$. Upper panel: the evolution of the maximal electron density as a function of $f(\mathcal{E}_b)\tau$ computed with the full nonlinear model (——) and by analytical solution (24) of the linearized problem (— · · —). Lower panel: the evolution of the maximal electric field enhancement $k = (\mathcal{E}_{max} - \mathcal{E}_b)/\mathcal{E}_b$ as a function of $f(\mathcal{E}_b)$). Solid lines: numerical solution of the full nonlinear model; dashed dotted lines: analytical approximation (29) where only the field of the electrons is accounted for and dashed lines: analytical approximation (52) of the total field.

ion cloud. For a more accurate estimate of the total field configuration, we refer to appendix B; there it is also shown that this will not significantly improve the estimate for the maximal field.

In figure 3 we compare the transition times given by equations (34) and (53) with numerically evaluated transition times. It shows that the approximation of similar electron and ion distributions leads to a very good approximation of the transition time. This figure also illustrates that the transition time $f\tau$ depends strongly on the electric field and increases for smaller fields. Moreover, looking at the transition time for higher diffusion coefficients, it is seen that diffusion tends to delay the transition to the streamer regime. This can be expected, since diffusion will tend to broaden the electron cloud, thereby suppressing space charge effects. Depending on the external parameters, the value of $\alpha d = f\tau$ at the transition can vary by a factor of two or more.

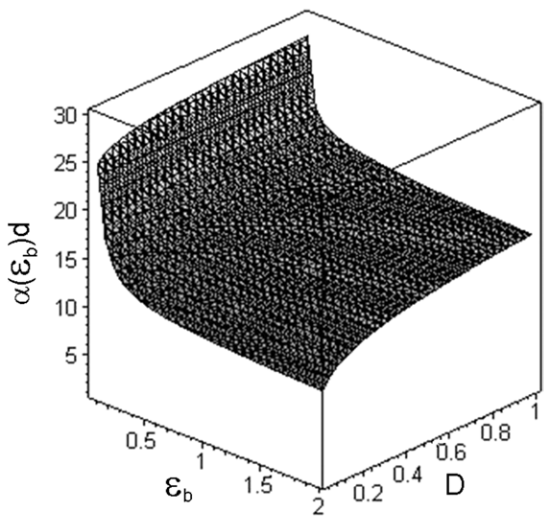

Figure 5. The transition distance αd of an electron avalanche in a non-attaching gas ($\nu = 0$) like N_2 or Ar in Townsend approximation (5) according to equation (53). It is shown as a function of background electric field $\mathcal{E}_b$ and diffusion coefficient D for initial parameter $\sigma_0 = 10^{-4}$ (accounting for one initial electron at normal pressure). The axes show dimensionless parameters, for dimensional parameters, see section 2. The values for $\alpha d = f\tau$ largely deviate from the Raether–Meek criterion (10).

4.5. The final results on the transition criterion

The transition time approximated by equation (53) as a function of both background electric field and diffusion coefficient is visualized as a 3-dimensional plot in figure 5. This figure shows that the Raether–Meek transition criterion, that stated that $f\tau = \alpha d$ takes an approximately constant value of 18 to 21, corresponds to the case of relatively high diffusion and background field. However, realistic values of D are smaller than unity, and a background electric field higher than 2 also seems unrealistic. So in the parameter range of real experiments, the correction given by equation (53) on the Raether–Meek criterion cannot be neglected.

We now discuss the particular example of an electron avalanche in (dry) air, for which coefficients different than in N_2 have to be used. In particular, the ionization length and field in air are given by [22] $\alpha_0 = 0.87\,\mu\mathrm{m}(N/N_0)$ and $E_0 = 277\,\mathrm{kV\,cm^{-1}} \cdot N/N_0$. For the values of the mobility and the diffusion coefficient of the electrons as a function of the electric field we use experimental values as well as numerical solutions of the Boltzmann equation (see appendix A). Inserting these in equation (53), we can compute

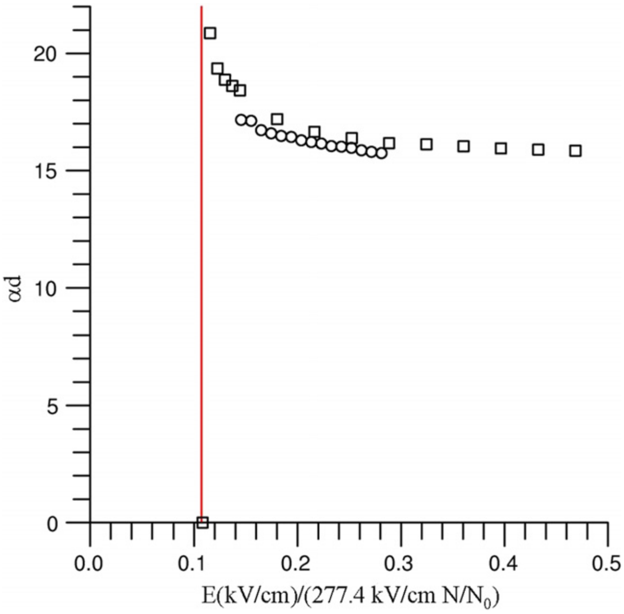

Figure 6. The transition value of αd in air as a function of the reduced electric field E_b/N. The vertical line indicates the field below which attachment overcomes ionization, and avalanches cannot grow anymore. (○): evaluated with experimental parameters for $\alpha(E)$ [35] and D_e/μ_e [36]; (□): evaluated with parameters from a Boltzmann solver [5].

the value of $\alpha(|\boldsymbol{E}|)d$ at the transition for different background fields as shown in figure 6. For large fields, the value of αd at transition saturates towards 16; the value grows with decreasing reduced field as long as $\mathcal{E} > 27.7\,\mathrm{kV\,cm^{-1}}$. At lower fields, attachment overcomes electron impact ionization, and a single electron cannot generate a streamer. Therefore, very large values of αd as in figure 5 are suppressed by electron attachment, see equation (8), and in air, αd increases from 15 to above 21 with decreasing field.

5. Summary and conclusions

In this paper, first the theory behind the Raether–Meek criterion for the avalanche-to-streamer transition was reviewed. Based on discharge simulations as shown in figure 1 and on physical and analytical considerations, it was argued that quantitative predictions require a diffusive correction to this criterion.

A dimensional analysis identified the characteristic length scales, which are a function of the neutral gas type and density. In particular, the dimensionless quantities $\alpha(\mathcal{E}_b)d$ and $D = D_e\alpha_0/(\mu_e E_0)$ have been extracted from the problem. The first expresses the distance d in multiples of the effective ionization length in the background field, while the latter gives the ratio between diffusive and advective transport of electrons. The two continuity equations (2) and (3) for the positive and negative ions can be reduced to one single equation (15), therefore further analysis is valid both for attaching gases like air or for non-attaching gases like N_2 or Ar.

During the avalanche phase, space charge effects are negligible. This implies that the problem can be linearized around the background field, making it well-suited for analytical treatment. Indeed, for an electron avalanche evolving in a homogeneous background electric field, a closed analytical expression for the density distribution of the electrons exists. Furthermore, we have shown that the electric field of the electron cloud during the avalanche phase can also be described by a closed analytical expression. This led to the derivation of a lower bound for the avalanche to streamer transition (34).

The estimate of the transition time was improved by taking the field generated by the ions into account. For the ion distribution and field, no closed analytical expression exists. However, we found that spatial moments of the distribution can be calculated to arbitrary order. A surprising result of this analysis is that the centre of mass of the ion cloud moves with the same velocity as that of the electron cloud, though the ions are immobile; the motion is therefore purely due to generation of additional ions. As could be expected, the ion cloud is more extended along the propagation direction and somewhat more compact in the lateral direction than the spherically symmetric electron cloud, cf sections 4.1 and 4.2 for more results and discussion.

For the field generated by the ions, a good approximation was developed. Then the sum of the electron and ion generated field compared with the background field lead to an analytical estimate for the avalanche-to-streamer transition (53) and (54). Our criterion for the transition is that the maximal relative field enhancement k has reached a value of approximately 3%. This value is based on comparing the analytical solution without space charge effects to the results of a numerical simulation of the full nonlinear problem and determining the moment of substantial deviations.

The transition distance αd strongly depends on diffusion D and on the background electric field. For high fields, the transition time saturates towards $\alpha d \simeq 15$. (We recall that the Raether–Meek-criterion stated that $\alpha d \simeq$ 18–21.) On the other hand, for low fields, when the processes are diffusion dominated, the avalanche lasts longer. In particular, in non-attaching gases like N_2 or Ar at low fields the relatively strong diffusion delays the transition considerably, even in terms of fixed αd (where even for fixed αd, the length $d \propto 1/\alpha$ can become very large for weak impact ionization α). Our dimensionless quantities enable us to translate the criterion given in (53) to any given gas type and density (54). For non-attaching gases in Townsend aproximation (5), the value of αd can be read off from figure 5. In air, attachment limits the emergence of a streamer in low fields, see equation (8). In this case, αd at the transition is in the range of 16 (for high background fields) to above 21 (for fields approaching E_k), cf figure 6. It is remarkable that in the end, the Raether–Meek criterion performs quite well for air, mainly because the attachment prevents streamer formation with large values of αd at very low fields. (We remark that the striations observed in [15] for very low fields are generic for atomic and non-attaching gases with essentially only elastic and ionizing collisions and only very few inelastic processes [37].)

The analytical models presented in this paper provide a useful tool to determine streamer formation. We stress that our transition criterion is based on the space charge effects to become significant. Our analysis relied on the linearization of the discharge equations on the background field. The nonlinear streamer propagation is the subject of other studies. In that phase the space charges and electric field strongly interact, and

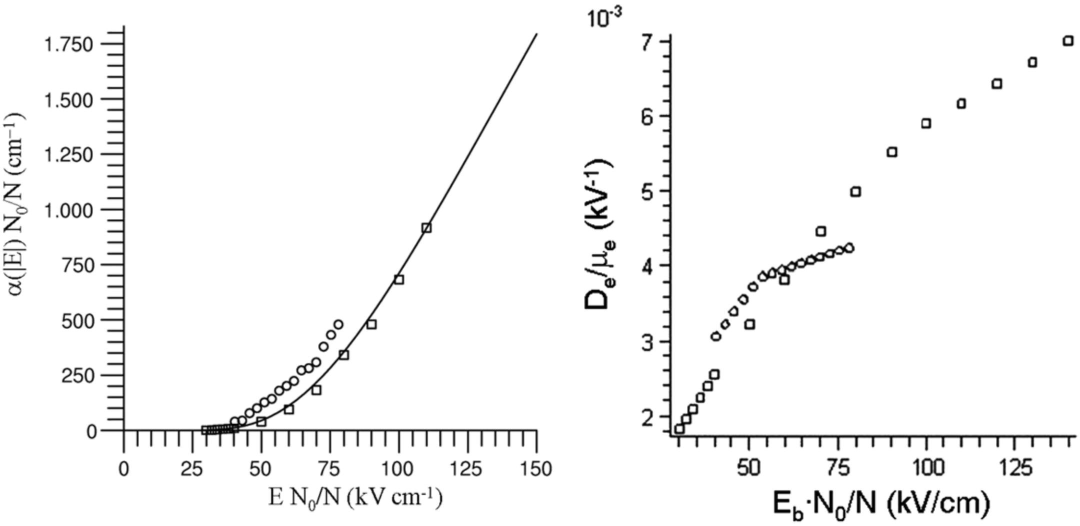

Figure A1. The ionization coefficient (left) and ratio of electron diffusion over mobility (right) in air, as a function of the reduced electric field. (○): experimental measurements (the values for α are taken from [35], the values for D/μ_e from [36]. (□): solution of the Boltzmann equation [5]. The solid line shows the ionization coefficient following the empirical formula (5) given in [22], with $\alpha_0 = 0.87\,\mu\text{m}(N/N_0)$ and $E_0 = 277\,\text{kV cm}^{-1} \cdot N/N_0$.

the analytical study of such streamers [38] is far more difficult than the analysis of the linear avalanche phase.

Acknowledgments

CM acknowledges a PhD grant of the Netherlands NWO/FOM-program on Computational Science.

Appendix A. Mobility and diffusion coefficients of electrons in air

To compute the transition criterion in air, we use the values for electron mobility and diffusion coefficient shown in figure A1. The left panel shows measured and calculated values of $\alpha(|E|)$, together with the fit $\alpha(|E|) = \alpha_0 \exp(-E_0/|E|)$. The experimental values are taken from the survey of electron swarm data by Dutton [35]. The computed values are the solution of the Boltzmann equation from [5]. Also, the empirical approximation of the ionization coefficient as a function of the background field as given by [22] is shown, $\alpha(|\boldsymbol{E}|) = \alpha_0 \exp(-E_0/|E|)$ with $\alpha_0 = 0.87\,\mu\text{m}(N/N_0)$ and $E_0 = 277\text{kV cm}^{-1} \cdot N/N_0$.

The values of D_e/μ_e as a function of the reduced electric field are given in the right plot of figure A1. Again, computed values from [5] are shown, as well as measured values from [36]. The value of the dimensionless diffusion coefficient D as a function of the electric field is easily derived from these figures.

Appendix B. A more accurate approximation for the ion density distribution

The simple approximation for the ion distribution ρ_1 in equation (49) leads to a relatively good approximation for the transition time in the case of a mid-gap transition. However, the real spatial distribution of ions is more narrow in the r-direction and wider and asymmetrical in the z-direction. In this appendix we present another approximation for the ion distribution, which will lead to a better overall approximation of the electric field induced by the ion trail and therefore of the total field distribution. However the price to pay for this is a much more complicated analytical expression for the density and the field.

A better approximation for ρ would be an ellipsoidal Gaussian distribution centred around $(r = 0, z = \langle z\rangle_\rho)$ with width $\langle z^2\rangle_\rho^c = \langle z^2\rangle_\rho - \langle z\rangle_\rho^2$ and $\langle r^2\rangle_\rho^c = \langle r^2\rangle_\rho$ in the z- and r-direction, respectively. The height of this Gaussian should be such that the total amount of ions at time t is still equal to $\sigma_0 e^{ft}$. The appropriate expression for the ion distribution is

$$\rho(r, z, t) = \frac{\sigma_0 \mathrm{e}^{ft}}{(2\pi)^{3/2} S_r^2 S_z} \exp\left[-r^2/(2S_r^2) - (z - \langle z\rangle_\rho)^2/(2S_z^2)\right]. \tag{B.1}$$

However, as far as we know, no closed analytical expression is known for the field of such an ellipsoidal Gaussian charge distribution. So instead, we take a spherical Gaussian distribution with the same height as the one defined in equation (B.1):

$$\rho_2(r, z, \tau) = \frac{\sigma_0 \mathrm{e}^{f\tau}}{(2\pi)^{3/2} S_\rho^3} \exp\left[-(r^2 + (z - \langle z\rangle_\rho)^2)/(2S_\rho^2)\right], \tag{B.2}$$

where

$$S_\rho^3 = \langle r^2\rangle_\rho^c \sqrt{\langle z^2\rangle_\rho^c} = \left(2D\left(\tau - \frac{1}{f}\right)\sqrt{2D\left(\tau - \frac{1}{f}\right) + \ell_\alpha^2}\right). \tag{B.3}$$

The electric field induced by this ion distribution is

$$E_{\rho_2}(r, z, \tau) = \frac{\sigma_0 \mathrm{e}^{f\tau}}{8\pi S_\rho^2} F\left(\sqrt{\frac{|\boldsymbol{s}_\rho|^2}{2S_\rho^2}}\right), \tag{B.4}$$

where $\boldsymbol{s}_\rho$ is defined in equation (51).

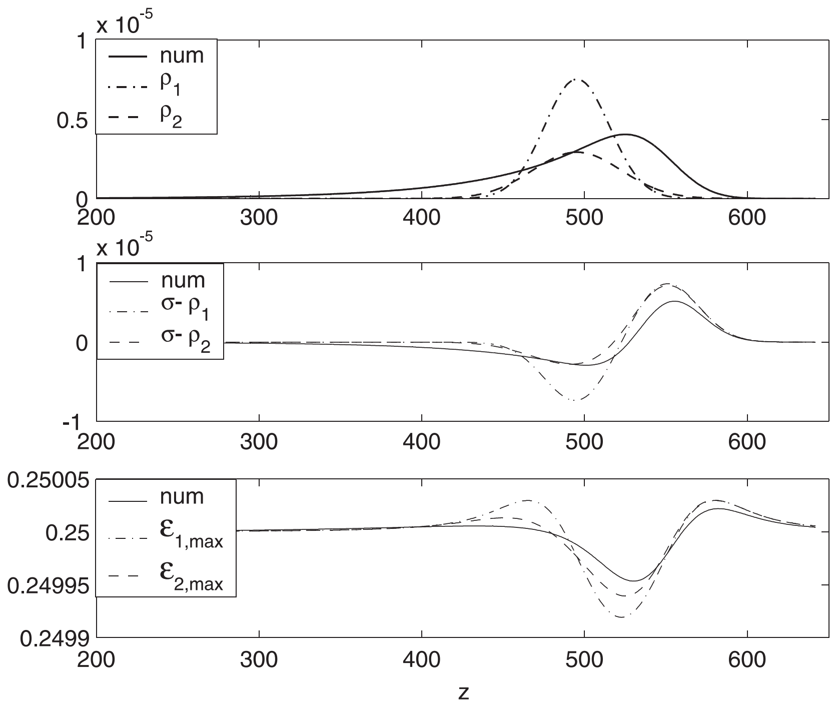

Figure B1. The ion density (upper figure), total charge density (middle figure) and electric field (lower figure) on the axis, computed with $E_0 = 0.25$, at $\tau = 2000$. The solid lines give the numerical solution, the dash-dotted lines the solution corresponding to ρ_1 and the dotted lines to ρ_2.

In figure B1 we compare the densities and fields given by the numerical solution and by the approximations ρ_1 and ρ_2. It is shown clearly that the approximation ρ_2 does not significantly improve the approximation ρ_1 for the field ahead of the electron cloud. This can be explained by the fact that the region ahead of the electron cloud contains very few ions, so that the ion generated field in this region is dominated by the distance to the ion cloud and by the total number of ions in the cloud, which are identical for ρ_1 and ρ_2. On the other hand, inside the ion cloud, the present approximation is much better. Therefore, while the results from section 4 approximate the maximal electric field and the transition time very well, the complete density distributions and fields up to this instant are better approximated by equations (23) and (B.2) for the electron and ion densities and by equations (26) and (B.4) for the respective electric fields.

References

[1] Mazur V, Krehbiel P R and Shao X 1995 Correlated high-speed video and radio interferometric observations of a cloud-to-ground lightning flash *J. Geophys. Res.* **100** 25731–54

[2] Bazelyan E M and Raizer Yu P 2000 *Lightning Physics and Lightning Protection* (Bristol: Institute of Physics Publishing)

[3] Gerken E A, InanU S and Barrington-Leigh C P 2000 Telescopic imaging of sprites *Geophys. Res. Lett.* **27** 2637

[4] Pasko V P and Stenbaek-Nielsen H C 2002 Diffuse and streamer regions of sprites *Geophys. Res. Lett.* **29** 82

[5] Liu N and Pasko V P 2004 Effects of photoionization on propagation and branching of positive and negative streamers in sprites *J. Geophys. Res.* **109** A04301

[6] Chen F F 1995 Industrial applications of low-temperature plasma physics *Phys. Plasmas* **2** 2164–75

[7] Eliasson B and Kogelschatz U 1991 Modeling and applications of silent discharge plasmas *IEEE Trans. Plasma Sci.* **19** 309–23

[8] Shimizu K, Kinoshita K, Yanagihara K, Rajanikanth B S, Katsura S and Mizuno A 1997 Pulsed-plasma treatment of polluted gas using wet-/low-temperature corona reactors *IEEE Trans. Plasma Sci.* **33** 1373–80

[9] Lisitsyn I V, Nomiyama H, Katsuki S and Akiyama H 1999 Streamer discharge reactor for water treatment by pulsed power *Rev. Sci. Instrum.* **70** 3457–62

[10] Winands G J J, Yan K, Nair A, Pemen A J M and van Heesch E J M 2005 Evaluation of corona plasma techniques for industrial applications: HPPS and DC/AC systems *Plasma Proc. Polymers* **2** 232–7

[11] Makarov M, Bonnet J and Pigache D 1998 High efficiency discharge-pumped XeCl laser *Appl. Phys.* B **66** 417–26

[12] Oda A, Sugawara H, Sakai Y and Akashi H 2000 Estimation of the light output power and efficiency of Xe barrier discharge excimer lamps using a one-dimensional fluid model for various voltage waveforms *J. Phys. D: Appl. Phys.* **33** 1507–13

[13] Kogelschatz U 2002 Industrial innovation based on fundamental physics *Plasma Sources Sci. Technol.* **11** A1–6

[14] Ebert U, Montijn C, Briels T M P, Hundsdorfer W, Meulenbroek B, Rocco A and van Veldhuizen E M 2006 The multiscale nature of streamers *Plasma Sources Sci. Technol.* **15** S118–29

[15] Dowds B J P, Barrett R K and Diver D A 2003 Streamer initiation in atmospheric pressure gas discharges by direct particle simulation *Phys. Rev.* E **68** 026412

[16] Phelps C T and Griffiths R F 1976 Dependence of positive corona streamer propagation on air pressure and water vapor content *J. Appl. Phys.* **47** 2929–34

[17] Kunhardt E E and Tzeng Y 1998 Development of an electron avalanche and its transition into streamers *Phys. Rev.* A **38** 1410–21

[18] Williams E R 2006 Problems in lightning physics—the role of the polarity asymmetry *Plasma Sources Sci. Technol.* **15** S91–108
[19] Dwyer J R 2003 A fundamental limit on electric fields in air *Geophys. Res. Lett.* **30** 2055
[20] Gurevich A V and Zybin K R 2005 Runaway breakdown and the mysteries of lightning *Physics Today* **58** 37–43
[21] Raether H 1939 The development of electron avalanche in a spark channel (from observations in a cloud chamber) *Z. Phys* **112** 464
[22] Raizer Y P 1991 *Gas Discharge Physics* (Berlin: Springer)
[23] Montijn C, Hundsdorfer W and Ebert U 2006 An adaptive grid method for the simulations of negative streamers in nitrogen *J. Comp. Phys.* at press (*Preprint* physics/0603070)
[24] Montijn C 2005 Evolution of negative streamers in nitrogen: a numerical investigation on adaptive grids *PhD Thesis* Technische Universiteit Eindhoven
[25] Montijn C, Ebert U and Hundsdorfer W 2006 Numerical convergence of the branching time of negative streamers *Phys. Rev.* E at press (*Preprint* physics/0604012)
[26] Meek J M A 1940 theory of spark discharge *Phys. Rev.* **57** 722–8
[27] Bazelyan E M and Raizer Yu P 1998 *Spark discharge* (New York: CRC Press)
[28] Loeb L B and Meek J M 1940 The mechanism of spark discharge in air at atmospheric pressure. I *J. Appl. Phys.* **11** 438–47
[29] Loeb L B and Meek J M 1940 The mechanism of spark discharge in air at atmospheric pressure II. *J. Appl. Phys.* **11** 459–74
[30] Ebert U, van Saarloos W and Caroli C 1997 Propagation and structure of planar streamer fronts *Phys. Rev.* E **55** 1530–49
[31] Rocco A, Ebert U and Hundsdorfer W 2002 Branching of negative streamers in free flight *Phys. Rev.* E **66** 035102
[32] Dhali S K and Williams P F 1987 Two-dimensional studies of streamers in gases *J. Appl. Phys.* **62** 4696–706
[33] Vitello P A, Penetrante B M and Bardsley J N 1994 Simulation of negative-streamer dynamics in nitrogen *Phys. Rev.* E **49** 5574–98
[34] Davies A J, Davies C S and Evans C J 1972 Computer simulation of rapidly developing gaseous discharges *Proc. IEE* **118** 816–23
[35] Dutton J 1975 A survey of electron swarm data *J. Phys. Chem. Ref. Data* **4** 664
[36] Lakshminarasimha C S and Lucas J 1977 The ratio of radial diffusion coefficient to mobility for electrons in helium, argon, air, methane and nitric oxide *J. Phys. D: Appl. Phys.* **10** 313–21
[37] Brok W M B 2005 Modelling of transient phenomena in gas discharges *PhD Thesis* Technische Universiteit Eindhoven
[38] Meulenbroek B, Rocco A and Ebert U 2004 Streamer branching rationalized by conformal mapping techniques *Phys. Rev.* E **69** 067402